Forward-bias diode parameters, electronic noise, and photoresponse of graphene/silicon Schottky junctions with an interfacial native oxide layer

Yanbin An,[1] Ashkan Behnam,[2] Eric Pop,[2,a)] Gijs Bosman,[1] and Ant Ural[1,b)]
[1]*Department of Electrical and Computer Engineering, University of Florida, Gainesville, Florida 32611, USA*
[2]*Department of Electrical and Computer Engineering, University of Illinois at Urbana-Champaign, Urbana, Illinois 61801, USA*

(Received 3 July 2015; accepted 5 September 2015; published online 21 September 2015)

Metal-semiconductor Schottky junction devices composed of chemical vapor deposition grown monolayer graphene on *p*-type silicon substrates are fabricated and characterized. Important diode parameters, such as the Schottky barrier height, ideality factor, and series resistance, are extracted from forward bias current-voltage characteristics using a previously established method modified to take into account the interfacial native oxide layer present at the graphene/silicon junction. It is found that the ideality factor can be substantially increased by the presence of the interfacial oxide layer. Furthermore, low frequency noise of graphene/silicon Schottky junctions under both forward and reverse bias is characterized. The noise is found to be 1/*f* dominated and the shot noise contribution is found to be negligible. The dependence of the 1/*f* noise on the forward and reverse current is also investigated. Finally, the photoresponse of graphene/silicon Schottky junctions is studied. The devices exhibit a peak responsivity of around 0.13 A/W and an external quantum efficiency higher than 25%. From the photoresponse and noise measurements, the bandwidth is extracted to be ~1 kHz and the normalized detectivity is calculated to be 1.2×10^9 cm $Hz^{1/2}$ W^{-1}. These results provide important insights for the future integration of graphene with silicon device technology. [http://dx.doi.org/10.1063/1.4931142]

I. INTRODUCTION

Graphene is an excellent candidate for next generation transparent and conductive electrodes due to its high transparency, good conductivity, high carrier mobility, mechanical flexibility, and two-dimensional planar geometry.[1–3] In particular, the demonstration of large-scale chemical vapor deposition (CVD) growth of monolayer graphene has opened up the possibility of large-scale production of graphene-based electronic and photonic devices.[4–6]

For most of these applications, interfaces and junctions play a significant role. Heterojunctions between graphene and conventional semiconductors combine the advantages of graphene with those of well-established semiconductor technology. Electronic and photonic devices based on graphene/silicon Schottky junctions, such as solar cells,[7–10] gas sensors,[11,12] a variable barrier diode called the "barristor,"[13] and photodetectors,[14–16] have recently been demonstrated. The solar cell application has attracted a significant amount of research interest since graphene can be used as a replacement for indium tin oxide (ITO). Power conversion efficiencies up to ~15% have recently been demonstrated.[9,10] The fact that the graphene Fermi level and hence the graphene/Si Schottky barrier height can be tuned either by electrostatic gating or by chemical doping constitutes the operational principle of devices such as gas sensors and the barristor.[11–13]

An important issue, which is much less explored, is the presence of an interfacial native oxide layer at the graphene/silicon junction. A few groups have pointed out the presence of an unintentional native oxide layer at the interface, which could grow either during the graphene transfer process or even after the silicon substrate is covered with graphene.[8–10,14,16] This interfacial native oxide layer has a thickness of 1–2 nm and results in a significant decrease in the reverse saturation current levels due to quantum tunneling.[16] It is also found to be responsible for the s-shaped kink frequently observed in the *I-V* curves of graphene/Si Schottky barrier solar cells.[10] However, most previous works have neglected the effect of this interfacial oxide layer on the diode parameters.

Furthermore, a systematic characterization of the electronic noise properties of graphene/Si Schottky junctions is currently lacking. For photodetector applications, which are much less explored compared to solar cells, electronic noise is critical since it determines important figures of merit such as the noise equivalent power (NEP) and the normalized detectivity. Most reports so far have simply assumed that shot noise is the major contributor to the total noise. The contribution of 1/*f* noise needs to be investigated in order to obtain more realistic performance figures for photodetectors based on graphene/silicon junctions.

In this paper, we experimentally characterize metal-semiconductor (MS) Schottky junction devices consisting of CVD-grown monolayer graphene on *p*-type silicon substrates, where graphene acts as the transparent, conductive metal electrode and silicon as the semiconductor. We extract the important Schottky diode parameters of this junction, such as barrier height, ideality factor, and series resistance

a)Present address: Department of Electrical Engineering, Stanford University, Stanford, California 94305, USA.
b)Author to whom correspondence should be addressed. Electronic mail: antural@ufl.edu

from room temperature forward-bias *I-V* characteristics by extending the method first proposed by Cheung and Cheung[17] to take into account the presence of an interfacial oxide layer. We compare the extracted values with those previously obtained from temperature-dependent reverse-bias *I-V* characteristics. We also discuss the effect of the interfacial oxide layer on the observed *I-V* characteristics. Furthermore, we measure the low frequency noise in these devices under both forward and reverse bias conditions. We find that 1/*f* noise is the major contributor to the total noise and that shot noise is negligible in the frequency range measured. We also study the dependence of 1/*f* noise on the DC current level. Furthermore, we characterize the photoresponse of these graphene/Si Schottky junctions and extract important parameters such as responsivity, noise equivalent power, bandwidth, and normalized detectivity based on the experimental data. Our results provide important insights into the electronic and optoelectronic properties of graphene/Si Schottky junctions.

II. EXPERIMENT

The graphene/*p*-type silicon Schottky junction devices were fabricated as described in detail previously.[16] Briefly, 1×10^{16} cm^{-3} doped *p*-type Si substrates with 300 nm thermal oxide were cleaned and windows were opened in the SiO_2 layer using a buffered oxide etch (BOE) to define the graphene/Si MS contact. Meanwhile, monolayer graphene was grown in a low pressure CVD system on a Cu foil and was transferred onto the Si substrate.[16] Inductively coupled plasma reactive ion etching (ICP-RIE) with O_2 was used to pattern the graphene into individual MS devices.[18] Finally, Ti/Au metal electrodes (5 nm/50 nm) were patterned on top of graphene for electrical probing. Figure 1(a) shows a 3D schematic of the fabricated graphene/Si Schottky junction device. Scanning electron microscope (SEM) image of a fabricated MS device is shown in Fig. 1(c). Figure 1(d) is the magnified view of the Si/SiO_2 edge with a 300 nm step, clearly showing that monolayer graphene provides excellent step coverage due to its high flexibility.

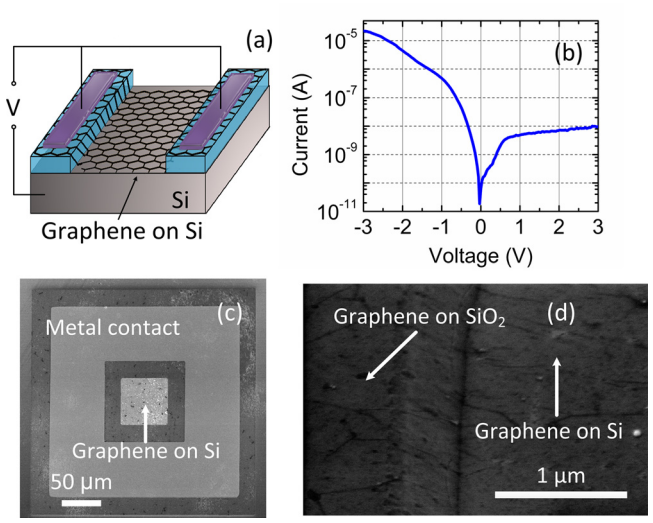

FIG. 1. (a) 3D schematic of the graphene/*p*-type silicon Schottky junction device. (b) *I-V* characteristics of a graphene/silicon device at room temperature. (c) Top-view scanning electron microscope (SEM) image of a fabricated graphene/silicon device. (d) Zoom-in of the SEM image at the SiO_2/Si edge with a step height of 300 nm, showing excellent step coverage of the monolayer graphene.

The DC electrical measurements of the devices were performed using a semiconductor parameter analyzer. For the study of electronic noise, a low noise battery and a low frequency, low noise current preamplifier were used in order to bias the device and amplify the noise signal. The noise measurements were performed by a spectrum analyzer. The time domain fluctuation data were collected by a digital data acquisition system. Photoresponse measurements were carried out using a tungsten-bromine white light source, an optical chopper, and a monochromator. The measurement setup is described in detail in Ref. 19.

III. RESULTS AND DISCUSSION

Figure 1(b) shows the room-temperature *I-V* characteristics of a graphene/Si Schottky junction device, depicting strong rectifying behavior. By studying the temperature dependence of the reverse saturation current, we have previously demonstrated that the electrical transport in the graphene/Si Schottky junctions is dominated by thermionic emission for temperatures above 260 K.[16] In thermionic emission, the *I-V* characteristics can be described by[20]

$$I = AA^{**}T^2 \exp\left(-\chi^{0.5}\delta\right)\exp\left(-\frac{\Phi_B}{kT}\right)\left[\exp\left(\frac{q(V-IR_s)}{nkT}\right)-1\right], \quad (1)$$

where A is the effective contact area, A^{**} is the reduced effective Richardson constant, T is absolute temperature, Φ_B is the Schottky barrier height, k is the Boltzmann constant, q is the magnitude of electronic charge, n is the ideality factor, and R_s is the series resistance. In our devices, a thin interfacial native oxide layer is present between graphene and silicon, which reduces the reverse saturation current due to quantum tunneling, as discussed in detail in Ref. 16. The transmission coefficient through this interfacial oxide layer can be described by the prefactor $\exp(-2(\frac{2m\chi}{\hbar^2})^{1/2}\delta)$, where m is the effective mass, $\hbar$ is the reduced Planck's constant, χ is the mean tunneling barrier height presented by the oxide, and δ is the interfacial oxide thickness.[21] Using χ in units of eV and δ in units of Å, the constants in the prefactor are approximately equal to 1, and the prefactor is typically written as $\exp(-\chi^{0.5}\delta)$, as given in Eq. (1).[21] Note that this transmission coefficient is assumed to be independent of bias.[21] This prefactor can be obtained by comparing the experimentally measured reverse saturation current and the theoretically calculated value,[16] which yields $\chi^{0.5}\delta \sim 9$ eV$^{0.5}$ Å.

Next, we extract the values of n, Φ_B, and R_s from the forward-bias *I-V* characteristics using a modified version of Cheung's method,[17] taking into account the interfacial oxide layer. This method enables the determination of these important Schottky diode parameters from a single forward-bias *I-V* measurement at a fixed temperature. Rearranging Eq. (1), we get[17]

$$V = R_s AJ + n\Phi_B + \frac{n}{\beta}\ln\left(\frac{J}{A^{**}T^2\exp(-\chi^{0.5}\delta)}\right), \quad (2)$$

where $J = I/A$ is the current density and $\beta = q/kT$. Taking the derivative of Eq. (2) and rearranging, we get[17]

$$\frac{dV}{d\ln J} = R_s AJ + \frac{n}{\beta}. \quad (3)$$

It can be seen from Eq. (3) that plotting $dV/d\ln J$ vs. J gives a straight line, where the series resistance R_s can be extracted from the slope and the ideality factor n from the y- intercept. $dV/d\ln J$ vs. J plot of a graphene/Si device is plotted by the blue data points in Fig. 2. From the linear fit indicated by the dashed line, we extract $n = 8.1$ and $R_s = 1.12\,\text{k}\Omega$. Extracting the ideality factor values using the same method from devices with different contact areas, we get an average value of $n = 8.9$. We can also define a function $H(J)$ as[17]

$$H(J) \equiv V - \frac{n}{\beta}\ln\left(\frac{J}{A^{**}T^2\exp(-\chi^{0.5}\delta)}\right) = R_s AJ + n\Phi_B. \quad (4)$$

A plot of $H(J)$ vs. J also gives a straight line, where the series resistance R_s can be extracted from the slope and the Schottky barrier height Φ_B from the y-intercept. The red data points in Fig. 2 show the $H(J)$ vs. J plot for the same device as in the $dV/d\ln J$ vs. J plot. The dashed line shows the linear fit of the experimental data, resulting in $\Phi_B = 0.47\,\text{eV}$ and $R_s = 1.14\,\text{k}\Omega$. Extracting the barrier height values using the same method from devices with different contact areas, we get a similar average value of $\Phi_B = 0.47\,\text{eV}$. The Schottky barrier height extracted from the forward-bias data using Cheung's method shows excellent agreement with the zero-bias barrier height value of 0.48 eV previously obtained by analyzing the temperature dependence of the reverse saturation current.[16] Furthermore, the series resistance value extracted from the $H(J)$ vs. J plot agrees very well with the value obtained from the $dV/d\ln J$ vs. J plot.

Values of n greater than unity could result due to several reasons: (1) Transport processes other than thermionic emission such as thermionic field emission, (2) image force lowering of the Schottky barrier, (3) a bias dependent Schottky barrier height due to the bias dependence of the graphene Fermi level, (4) Schottky barrier inhomogeneities[22,23] due to charge puddles on graphene, which have been experimentally observed recently at graphene/silicon carbide junctions,[24] and (5) the presence of the interfacial oxide layer.[25,26] The first two factors typically result in an ideality factor close to 1, and as discussed below, the third factor can be neglected under forward bias, leaving Schottky barrier inhomogeneities and the presence of the interfacial native oxide layer as the major contributors to the large n values observed in our devices.

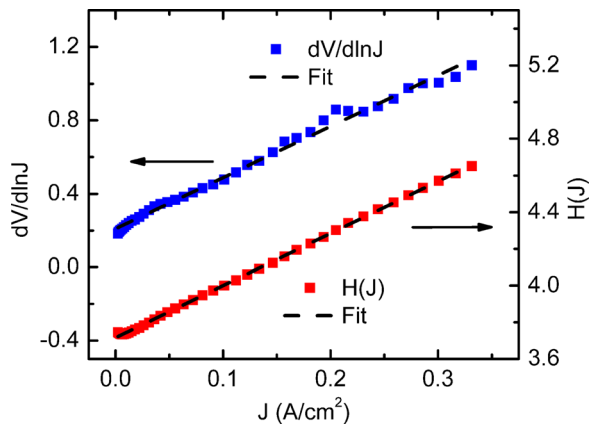

FIG. 2. Plots of $dV/d\ln J$ (left y-axis) and $H(J)$ (right y-axis) as a function of current density J calculated from forward bias I-V characteristics of the graphene/Si device using the equations in the text. The dashed lines show the linear fits to the experimental data.

Now, we consider the effect of the interfacial layer in more detail. The forward-bias voltage V consists of two components: The voltage across the interfacial layer V_i and the voltage across the depletion region of the semiconductor. The ideality factor due to the interfacial layer is given by $\frac{1}{n} = 1 - \frac{dV_i}{dV}$.[21,26] The change of the voltage across the interfacial layer with applied bias, dV_i/dV, is also affected by the presence of interface states and surface fixed charge. As a result, the ideality factor can be substantially increased by the presence of the interfacial oxide layer.[21,26] The ideality factors reported in the literature for graphene on both n-type and p-type Si substrates range from 1.08 to 33.5.[27,28] Recently, it was shown that etching the top layer of the copper foil used as the substrate in graphene growth minimizes metallic impurities and results in n values close to 1.[27] The wide range of n values reported in the literature could be attributed to the fluctuations in the interfacial layer properties such as the interfacial layer thickness, interface states, surface fixed charge, and impurities. This implies that the electronic properties of the graphene/Si Schottky junctions could be improved by optimizing the processing and fabrication conditions.

Next, we discuss the modulation of the graphene Fermi level with applied bias. Unlike conventional metals, the low density of states in graphene leads to the modulation of the graphene Fermi level and hence the Schottky barrier height Φ_B with applied bias.[16,29,30] The change in the depletion charge in silicon with applied bias leads to an equal and opposite change in the charge induced in graphene, which then shifts the graphene Fermi level.[16] This modulation becomes most pronounced under high reverse bias. However, under forward bias, a large change is not expected since the actual voltage drop across the junction is small. For our devices, the change in the Schottky barrier height under forward bias is estimated to be no more than a few meV. As a result, the effect of the bias dependence of the graphene Fermi level can be neglected under forward bias, as mentioned above.

We also performed noise measurements on the graphene/Si Schottky devices at various values of forward and reverse bias. Schottky junction devices are widely used as key components for signal detection and mixing. Therefore, in addition to the diode parameters extracted from I-V data, electronic noise and fluctuations in these devices are also of critical importance.[31–33] Study of low frequency excess noise plays a significant role not only because it is one of the key parameters that limit the overall device performance but also it is a powerful tool to probe and understand the electronic transport in these devices.

Figures 3(a) and 3(b) show the current noise power spectral density S_I of a graphene/Si device at bias magnitudes ranging from 1 V to 2.5 V under forward and reverse bias, respectively. As we can see from the figures, the noise spectra in both forward and reverse bias show 1/*f*-type behavior. 1/*f* noise, which has been widely observed in both bulk semiconductors and junctions, can be described by the following equation:[32]

$$S_I = \frac{\alpha \cdot I^{\beta}}{f^{\gamma}}, \tag{5}$$

where α is the noise amplitude, I is the DC current, f is frequency, and β and γ are constant exponents. Power law fits to the experimental data show that for forward bias [Fig. 3(a)], $\gamma = 1.12$–1.18, and for reverse bias [Fig. 3(b)], $\gamma = 1.14$–1.21. The extracted γ values close to 1 confirm the 1/*f*-type noise behavior.

Shot noise is also frequently observed in Schottky diodes with a constant spectral density given by $S_I^{shot} = 2qI$, where q is the electronic charge. For the values of I in our devices, S_I^{shot} is much smaller than the 1/*f* noise in the frequency range measured. As a result, the shot noise contribution can be neglected and the total noise in these devices is 1/*f*-limited.

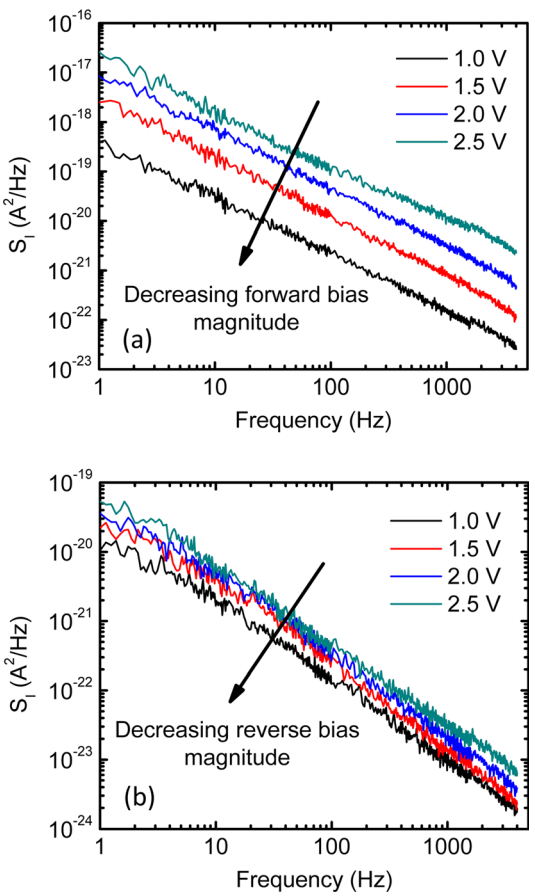

FIG. 3. Current noise spectral density of the graphene/silicon Schottky junction device measured at different voltage magnitudes as labeled in the plots, under (a) forward-bias and (b) reverse-bias, showing that the noise is 1/*f* limited in both cases.

We further studied the current dependence of S_I, which is shown in Fig. 4 as the red and blue points for forward and reverse bias, respectively. For forward bias, the power law fit results in $\beta = 1.19$. This extracted β value agrees with the theoretical model of 1/*f* noise in forward-biased Schottky barrier diodes operating in the thermionic emission mode, which approximately predicts $S_I \propto I$.[33] This model, which attributes noise to carrier mobility fluctuations within the depletion region, has been proven to be valid in forward-biased Schottky junctions composed of other materials, as well.[34,35] However, for reverse bias, the power law fit to the experimental data yields $\beta = 2.20$. This could be explained by Schottky barrier height fluctuations due to carrier trapping and de-trapping, which has been shown to yield $S_I \propto I^2$.[31] A similar current dependence has been observed for reverse-biased carbon nanotube film-silicon Schottky junctions.[19]

Finally, we characterized the photoresponse of reverse-biased graphene/Si Schottky devices. The responsivity R of a photodetector is defined as the photocurrent generated per unit incident optical power, i.e., $R = I_{photo}/P_{inc}$. Figure 5(a) shows the spectral responsivity of a graphene/Si device in the visible and near-infrared region at a reverse bias magnitude of 1 V. As we can see from the figure, the peak responsivity of the device is about 0.13 A/W. The dotted lines in the figure correspond to various values of the external quantum efficiency (QE) of the photodetector (in percent) defined as $\eta_{ext} = \frac{124 \times R}{\lambda}$, where R is the responsivity in units of A/W and λ is the wavelength of the incident light in units of μm. As we can see from the figure, the peak quantum efficiency of the device is higher than 25%. These responsivity and QE values are similar to those reported for graphene-based photovoltaic detectors,[14,15,36–38] as well as Schottky barrier photodetectors based on other materials such as AlGaN, GaN, and ZnO.[39–42] Furthermore, both the responsivity and the quantum efficiency of graphene/Si Schottky junction devices are higher than those of carbon nanotube film/Si Schottky devices reported previously.[19] The main factors limiting the

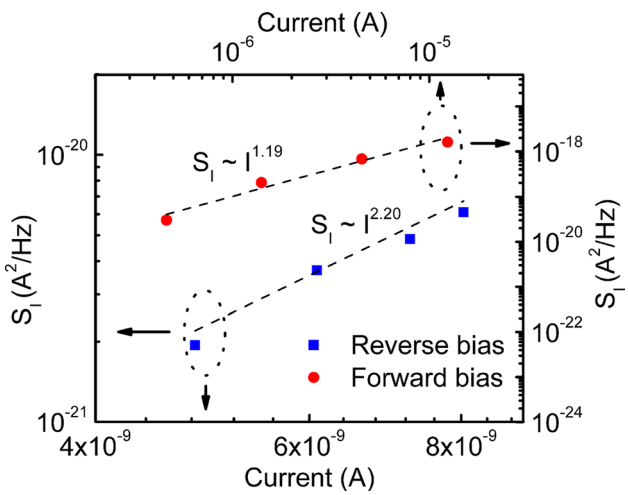

FIG. 4. S_I as a function of the DC current I measured at 10 Hz for both forward-bias (red circles, right y-axis, top x-axis) and reverse-bias (blue squares, left y-axis, bottom x-axis). The dashed lines show the power-law fits to the experimental data, resulting in exponents of 1.19 and 2.20 for forward and reverse bias, respectively.

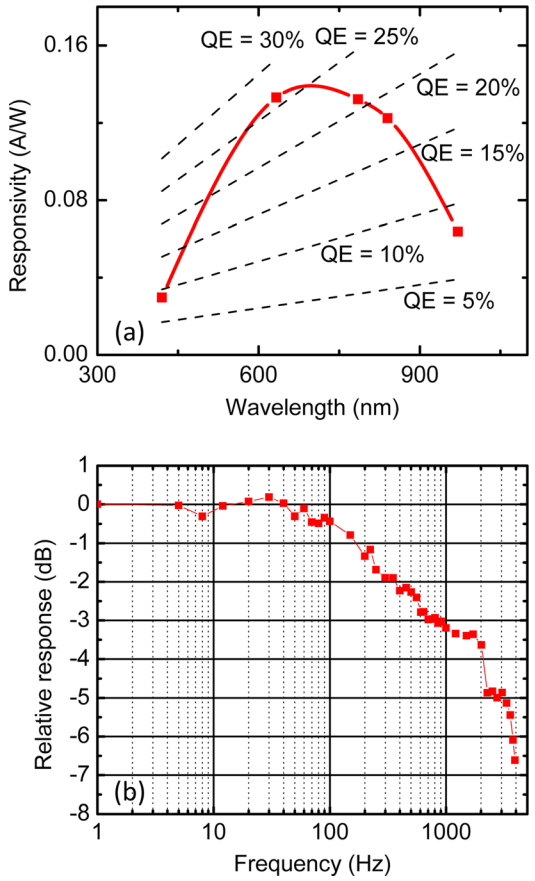

FIG. 5. (a) Spectral responsivity of a graphene/Si device at a reverse bias magnitude of 1 V, showing a peak responsivity value of about 0.13 A/W. The solid line is a guide for the eye and the dashed lines show various external quantum efficiency (QE) values ranging from 5% to 30%. (b) Relative photoresponse spectrum of the same graphene/silicon device as in part (a), as a function of the optical chopper frequency at a reverse bias magnitude of 1 V and an incident wavelength of 633 nm.

responsivity of the graphene/Si Schottky junctions are reflection at the top surface of the device, recombination of the generated electron-hole pairs, particularly at the graphene/silicon interface, and absorption of photons outside of the depletion region. The responsivity could be increased by using an antireflection coating, improving the interface properties, and optimizing the silicon substrate doping.

We also characterized the relative photoresponse of our devices at different optical chopper frequencies, which we define as $G_{dB} = 20\log_{10}(R_f/R_0)$, where R_f and R_0 are the responsivity at a chopper frequency of f and at steady-state ($f = 0$), respectively. The spectral relative photoresponse of the graphene/Si device in Fig. 5(a) is shown in Fig. 5(b) at a reverse bias magnitude of 1 V and an incident wavelength of 633 nm. The bandwidth B of the photodetector can be estimated as the frequency at which the level of the relative photoresponse is -3 dB. From Fig. 5(b), this corresponds to a bandwidth of $B \sim 1$ kHz. This value of the bandwidth is comparable to or slightly better than other graphene-based photovoltaic detectors[14,15,36–38] and is significantly higher than that of the photodetector fabricated with CNT film/Si Schottky junctions.[19] However, it is worth noting that this bandwidth is still lower than conventional silicon *p-n* or Schottky junction photodetectors. This could be due to defects and traps at the graphene/Si interface introduced during the fabrication process. The interfacial native oxide layer could also be a contributing factor to the low bandwidth.[19,43] This implies that the bandwidth of the graphene/Si Schottky junction photodetectors could be improved by further optimizing and controlling the processing and fabrication conditions.

Another important figure of merit for a photodetector is the NEP, which is a measure of the minimum detectable signal. NEP is defined as the incident optical power required to produce a signal to noise ratio of unity in a bandwidth of 1 Hz, given by

$$\mathrm{NEP} = \frac{\sqrt{\langle i^2 \rangle}}{R}, \tag{6}$$

where R is the responsivity and $\langle i^2 \rangle$ is the total square noise current. Neglecting the noise below 1 Hz (which is not measured), the latter is given by[39,40,42]

$$\langle i^2 \rangle \approx \int_1^B S_I(f)df, \tag{7}$$

where S_I is given by Eq. (5) and B is the bandwidth. By integrating the power law fit to the experimental S_I data of Fig. 3(b), we get $\mathrm{NEP} = 2.6 \times 10^{-9}$ W at 1 V reverse bias and 633 nm incident light. Finally, the normalized detectivity of the graphene/Si Schottky junction photodetector can be calculated from

$$D^* = \frac{\sqrt{A}\sqrt{B}}{NEP}, \tag{8}$$

where A is the effective device area. The calculated detectivity of the graphene/Si device is 1.2×10^9 cm Hz$^{1/2}$ W^{-1}, which is higher than that of the photodetector fabricated with CNT film/Si Schottky junctions.[19] It is worth emphasizing that, in previous work on graphene-based photovoltaic detectors, NEP and D^* values have almost always been calculated by assuming that shot noise is the major contributor to the total noise,[15,36,38] which results in much lower NEP and much higher D^* values. As we have shown, $1/f$ noise dominates the total noise in these devices, and hence the NEP and D^* values quoted in previous work are more optimistic than experimentally observed.

IV. CONCLUSIONS

In conclusion, we fabricated and characterized the electronic and optoelectronic properties of CVD-grown monolayer graphene/*p*-type silicon metal-semiconductor Schottky junctions. The values of the ideality factor, Schottky barrier height, and series resistance were extracted using Cheung's method modified to take into account the interfacial native oxide layer between graphene and silicon. It was found that the ideality factor n can be substantially increased by the presence of the interfacial oxide layer. Low frequency noise, under both forward and reverse bias, exhibited $1/f$ limited behavior, and the shot noise contribution was found to be

negligible in the frequency range measured. The forward-bias current noise showed $S_I \propto I$ dependence, which agrees with the theoretical model of $1/f$ noise for forward-biased Schottky diodes operating in the thermionic emission mode. The reverse-bias current noise showed $S_I \propto I^2$ dependence, suggesting that barrier height fluctuations start to play an important role under reverse bias. The spectral photoresponse of the device exhibited a peak responsivity of around 0.13 A/W and external quantum efficiency higher than 25%. The bandwidth of the photodetector was extracted to be $\sim$1 kHz from the measurements of the relative photoresponse spectrum using an optical chopper. Using the results from the noise and photoresponse measurements, the normalized detectivity was calculated to be 1.2×10^9 cm $\mathrm{Hz}^{1/2}$ W^{-1}. These results provide important insights into the electronic and optoelectronic properties of graphene/Si Schottky junctions and the interfacial oxide layer that could be present between graphene and silicon. These results also show that graphene holds promise as a transparent and conductive electrode compatible with silicon technology and that there is significant room for improvement by optimizing the processing and fabrication conditions.

ACKNOWLEDGMENTS

This work was funded by the Research Opportunity Seed Fund.

[1]K. S. Novoselov, A. K. Geim, S. V. Morozov, D. Jiang, Y. Zhang, S. V. Dubonos, I. V. Grigorieva, and A. A. Firsov, Science **306**, 666 (2004).
[2]K. S. Novoselov, A. K. Geim, S. V. Morozov, D. Jiang, M. I. Katsnelson, I. V. Grigorieva, S. V. Dubonos, and A. A. Firsov, Nature **438**, 197 (2005).
[3]K. S. Kim, Y. Zhao, H. Jang, S. Y. Lee, J. M. Kim, K. S. Kim, J.-H. Ahn, P. Kim, J.-Y. Choi, and B. H. Hong, Nature **457**, 706 (2009).
[4]X. Li, W. Cai, J. An, S. Kim, J. Nah, D. Yang, R. Piner, A. Velamakanni, I. Jung, E. Tutuc, S. K. Banerjee, L. Colombo, and R. S. Ruoff, Science **324**, 1312 (2009).
[5]S. Bae, H. Kim, Y. Lee, X. Xu, J.-S. Park, Y. Zheng, J. Balakrishnan, T. Lei, H. Ri Kim, Y. I. Song, Y.-J. Kim, K. S. Kim, B. Ozyilmaz, J.-H. Ahn, B. H. Hong, and S. Iijima, Nat. Nanotechnol. **5**, 574 (2010).
[6]Z. Yan, J. Lin, Z. Peng, Z. Sun, Y. Zhu, L. Li, C. Xiang, E. L. Samuel, C. Kittrell, and J. M. Tour, ACS Nano **6**, 9110 (2012).
[7]X. Li, H. Zhu, K. Wang, A. Cao, J. Wei, C. Li, Y. Jia, Z. Li, X. Li, and D. Wu, Adv. Mater. **22**, 2743 (2010).
[8]X. Miao, S. Tongay, M. K. Petterson, K. Berke, A. G. Rinzler, B. R. Appleton, and A. F. Hebard, Nano Lett. **12**, 2745 (2012).
[9]E. Shi, H. Li, L. Yang, L. Zhang, Z. Li, P. Li, Y. Shang, S. Wu, X. Li, J. Wei, K. Wang, H. Zhu, D. Wu, Y. Fang, and A. Cao, Nano Lett. **13**, 1776 (2013).
[10]Y. Song, X. Li, C. Mackin, X. Zhang, W. Fang, T. Palacios, H. Zhu, and J. Kong, Nano Lett. **15**, 2104 (2015).
[11]H. Kim, K. Lee, N. McEvoy, C. Yim, and G. S. Duesberg, Nano Lett. **13**, 2182 (2013).
[12]M. A. Uddin, A. K. Singh, T. S. Sudarshan, and G. Koley, Nanotechnol. **25**, 125501 (2014).
[13]H. Yang, J. Heo, S. Park, H. J. Song, D. H. Seo, K.-E. Byun, P. Kim, I. Yoo, H.-J. Chung, and K. Kim, Science **336**, 1140 (2012).
[14]X. An, F. Liu, Y. J. Jung, and S. Kar, Nano Lett. **13**, 909 (2013).
[15]P. Lv, X. Zhang, X. Zhang, W. Deng, and J. Jie, IEEE Electron. Device Lett. **34**, 1337 (2013).
[16]Y. An, A. Behnam, E. Pop, and A. Ural, Appl. Phys. Lett. **102**, 013110 (2013).
[17]S. K. Cheung and N. W. Cheung, Appl. Phys. Lett. **49**, 85 (1986).
[18]A. Behnam, Y. Choi, L. Noriega, Z. Wu, I. Kravchenko, A. G. Rinzler, and A. Ural, J. Vac. Sci. Technol. B **25**, 348 (2007).
[19]Y. An, H. Rao, G. Bosman, and A. Ural, J. Vac. Sci. Technol. B **30**, 021805 (2012).
[20]S. M. Sze, *Physics of Semiconductor Devices* (Wiley, 1981).
[21]H. C. Card and E. H. Rhoderick, J. Phys. D: Appl. Phys. **4**, 1589 (1971).
[22]J. H. Werner and H. H. Guttler, J. Appl. Phys. **69**, 1522 (1991).
[23]S. Chand and J. Kumar, J. Appl. Phys. **82**, 5005 (1997).
[24]S. Shivaraman, L. H. Herman, F. Rana, J. Park, and M. G. Spencer, Appl. Phys. Lett. **100**, 183112 (2012).
[25]R. T. Tung, Mater. Sci. Eng. R **35**, 1 (2001).
[26]C.-Y. Wu, J. Appl. Phys. **51**, 3786 (1980).
[27]D. Sinha and J. U. Lee, Nano Lett. **14**, 4660 (2014).
[28]C.-C. Chen, M. Akyol, C.-C. Chang, A. F. J. Levi, and S. B. Cronin, Nano Lett. **11**, 1863 (2011).
[29]S. Tongay, M. Lemaitre, X. Miao, B. Gila, B. R. Appleton, and A. F. Hebard, Phys. Rev. X **2**, 011002 (2012).
[30]J. Chauhan, A. Rinzler, and J. Guo, J. Appl. Phys.**112**, 104502 (2012).
[31]S. T. Hsu, IEEE Trans. Electron Devices **17**, 496 (1970).
[32]T. G. M. Kleinpenning, Solid-State Electron. **22**, 121 (1979).
[33]M.-Y. Luo, G. Bosman, A. Van der Ziel, and L. L. Hench, IEEE Trans. Electron Devices **35**, 1351 (1988).
[34]N. A. Hastas, C. A. Dimitriadis, L. Dozsa, E. Gombia, and R. Mosca, J. Appl. Phys. **96**, 5735 (2004).
[35]Y. An, H. Rao, G. Bosman, and A. Ural, Appl. Phys. Lett. **100**, 213102 (2012).
[36]L.-H. Zeng, M.-Z. Wang, H. Hu, B. Nie, Y.-Q. yu, C.-Y. Wu, L. Wang, J.-G. Hu, C. Xie, F.-X. Liang, and L.-B. Luo, ACS Appl. Mater. Interfaces **5**, 9362 (2013).
[37]M. E. Ayhan, G. Kalita, M. Kondo, and M. Tanemura, RSC Adv. **4**, 26866 (2014).
[38]M. Zhu, X. Li, Y. Guo, X. Li, P. Sun, X. Zang, K. Wang, M. Zhong, D. Wu, and H. Zhu, Nanoscale **6**, 4909 (2014).
[39]Q. Chen, J. W. Yang, A. Osinsky, S. Gangopadhyay, B. Lim, M. Z. Anwar, M. A. Khan, D. Kuksenkov, and H. Temkin, Appl. Phys. Lett. **70**, 2277 (1997).
[40]A. Osinsky, S. Gangopadhyay, B. W. Lim, M. Z. Anwar, M. A. Khan, D. V. Kuksenkov, and H. Temkin, Appl. Phys. Lett. **72**, 742 (1998).
[41]A. Osinsky, S. Gangopadhyay, J. W. Yang, R. Gaska, D. Kuksenkov, H. Temkin, I. K. Shmagin, Y. C. Chang, J. F. Muth, and R. M. Kolbas, Appl. Phys. Lett. **72**, 551 (1998).
[42]S. J. Young, L. W. Ji, S. J. Chang, and Y. K. Su, J. Cryst. Growth **293**, 43 (2006).
[43]M. C. Putnam, D. B. Turner-Evans, M. D. Kelzenberg, S. W. Boettcher, N. S. Lewis, and H. A. Atwater, Appl. Phys. Lett. **95**, 163116 (2009).